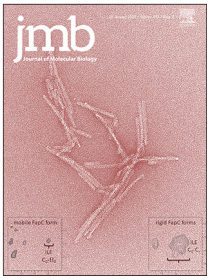

ATP Impedes the Inhibitory Effect of Hsp90 on $A\beta_{40}$ Fibrillation

Hongzhi Wang [1], Max Lallemang [2,3], Bianca Hermann [2], Cecilia Wallin [4], Rolf Loch [1], Alain Blanc [5], Bizan N. Balzer [2,3], Thorsten Hugel [2,3] and Jinghui Luo [1]*

*1 - **Department of Biology and Chemistry,** Paul Scherrer Institute, 5232 Villigen, Switzerland*
*2 - **Institute of Physical Chemistry,** University of Freiburg, Albertstraße 21, 79104 Freiburg, Germany*
*3 - **Cluster of Excellence livMatS @ FIT – Freiburg Center for Interactive Materials and Bioinspired Technologies,** University of Freiburg, Georges-Köhler-Allee 105, D-79110 Freiburg, Germany*
*4 - **Department of Biochemistry and Biophysics,** Stockholm University, 10691 Stockholm, Sweden*
*5 - **Center for Radiopharmaceutical Sciences,** Paul Scherrer Institute, 5232 Villigen, Switzerland*

***Correspondence to Jinghui Luo:** Jinghui.luo@psi.ch (J. Luo)*
https://doi.org/10.1016/j.jmb.2020.11.016
Edited by J. Buchner

Abstract

Heat shock protein 90 (Hsp90) is a molecular chaperone that assists protein folding in an Adenosine triphosphate (ATP)-dependent way. Hsp90 has been reported to interact with Alzheimer´s disease associated amyloid-β (Aβ) peptides and to suppress toxic oligomer- and fibril formation. However, the mechanism remains largely unclear. Here we use a combination of atomic force microscopy (AFM) imaging, circular dichroism (CD) spectroscopy and biochemical analysis to quantify this interaction and put forward a microscopic picture including rate constants for the different transitions towards fibrillation. We show that Hsp90 binds to $A\beta_{40}$ monomers weakly but inhibits $A\beta_{40}$ from growing into fibrils at substoichiometric concentrations. ATP impedes this interaction, presumably by modulating Hsp90's conformational dynamics and reducing its hydrophobic surface. Altogether, these results might indicate alternative ways to prevent $A\beta_{40}$ fibrillation by manipulating chaperones that are already abundant in the brain.

Introduction

Heat shock protein 90 (Hsp90) is a ubiquitously expressed, evolutionarily conserved, and highly dynamic molecular chaperone, which mainly consists of three structural domains: an N-terminal ATP-binding domain, a middle domain for client protein binding, and a C-terminal dimerization domain.[1] Hsp90, including yeast Hsp90 (Hsp82) used in this study (Table S1), usually locate intracellularly,[2,3] but can also be secreted into extracellular space.[4] It participates in a variety of cellular processes including cell survival, hormone signaling, cell cycle control and response to cellular (heat) stress,[5–9] as well as in assisting folding, maturation and degradation of more than 200 'client proteins' in eukaryotes.[10–13] These functions of Hsp90 are achieved in concert with different co-chaperones and adaptor proteins and often with the help of ATP.[8,14]

Amyloid-β (Aβ) peptide fibrillation and accumulation are usually triggered by a conformational transition from random coil to β-sheet secondary structures and progresses via the classical lag-, elongation-, and plateau-phases, in which hydrophobic interactions are involved.[15,16,75] These processes usually take place extracellularly and play central roles in the progression of Alzheimer's disease according to the amyloid cascade hypothesis.[15,17] However, Aβ can be

produced intracellularly or taken up from extracellular space to the cytoplasm through receptor binding and subsequent internalization and accumulates intracellularly including in mitochondria.[18] Intracellular Aβ accumulation influences a variety of physiological activities like autophagy, degradation and apoptosis, indicative of the crucial role of intracellular Aβ in Alzheimer's disease.[19,20] Recent evidence suggests that lipid raft and lipid membranes play crucial roles in Alzheimer's disease by promoting the production and oligomer formation of Aβ peptides, while Aβ oligomers can bind to lipid membranes and induce the aberrant clustering of lipid raft and membranes.[21,22] As the disease progresses, intracellular Aβ oligomers may interact with lipid membranes, induce neuronal dysfunction, or pass into the extracellular space as a source of fibril deposits.[18] Changes in the raft-lipid composition or membranes of the cells can induce the release of heat shock proteins, like Hsp90, from cytoplasm to modulate intercellular signalling.[23,24] *In vivo* studies indicate that intracellular chaperones can play a role in modulating intracellular Aβ metabolism and toxicity.[25] Thus interactions between Hsp90 and Aβ can possibly take place both extracellularly and intracellularly, while Aβ aggregation mainly occur extracellularly. The *In vivo* interaction between Hsp90 and Aβ and the physiological relevance of this interaction remain to be explored. Molecular chaperones such as Hsp90 are in the first line of the cellular defense system against protein aggregation. A growing body of evidence indicates that Hsp90 inhibits amyloid protein aggregation, cellular toxicity, or clearance of Alzheimer's Aβ,[10,26–29] but the molecular mechanism of Hsp90 modulating Aβ remains unknown. For instance, does Hsp90 interfere with Aβ fibrillation in an ATP-dependent and/or specific way? How do different Hsp90 conformations influence Aβ fibrillation? In which phase does Hsp90 interfere with Aβ fibrillation?

To answer these questions, we investigated how $A\beta_{40}$ fibrillation is affected by dimeric wild type Hsp90 (WT), Hsp90 tetramer, and the ATPase defective mutant E33A also lacking the charged linker region between the N-terminal and middle domains.[30] We assumed that each one has a different dynamics in equilibrium, therefore exposing varied time-dependent hydrophobic surfaces as possible client binding sites. The fibrillation of Aβ was observed with atomic force microscopy (AFM) imaging under various environmental conditions, by Thioflavin T (ThT) fluorescence, circular dichroism (CD) spectroscopy and SDS-PAGE. AFM imaging has already revealed a variety of structural information about $A\beta_{40}$ aggregation[31–34] and its interaction with small molecules.[35–37] Furthermore, AFM imaging was also previously used to support that the chaperones Hsp60[38], GroEL[39] and HspB1[40] inhibit $A\beta_{40}$ aggregation. However, to the best of our knowledge neither the role of Hsp90 on the $A\beta_{40}$ aggregation, nor the effect of ATP on this system have been studied by AFM experiments yet. In addition, our specific modulation of Hsp90 allows us to put forward a mechanism for the inhibition of fibril growth. We observed that all three Hsp90 forms inhibit $A\beta_{40}$ fibrillation to different degrees and this effect of Hsp90 can be impeded by the addition of ATP, which can induce a change in the conformation dynamics and hydrophobicity of Hsp90. We therefore suggest that Hsp90 inhibits $A\beta_{40}$ fibrillation through the modulation of conformational dynamics and hydrophobic surfaces. Our results provide a new perspective for the mechanism of inhibition of amyloid fibrillation by Hsp90 and other chaperones.

Results

Hsp90 inhibits $A\beta_{40}$ fibrillation

We used AFM in air to investigate the morphology changes of the $A\beta_{40}$ peptides in the absence or presence of Hsp90 dimers (wild type), tetramers, and an ATPase-deficient E33A mutant. Figure 1 shows the AFM images recorded after an incubation of 10 μM $A\beta_{40}$ alone or with 0.5 μM Hsp90 variants at 37 °C for 24 h. The $A\beta_{40}$ sample alone forms fibrils in an unbranched, twisted helical morphology while the $A\beta_{40}$ samples in the presence of three Hsp90 forms display other distinct morphologies. In the presence of Hsp90 proteins, the $A\beta_{40}$ peptides aggregated into irregular small amorphous aggregates. Likely, the larger $A\beta_{40}$ aggregates observed in the presence of the Hsp90 tetramer may result from the co-aggregation with the $A\beta_{40}$ peptides and the aggregation-prone tetramer. This result indicates that Hsp90 proteins suppress the formation of $A\beta_{40}$ fibrils, but to different degrees depending on their forms, WT induced the formation of smaller amorphous aggregates compared with tetramer and E33A, suggesting that WT is probably the most efficient one to inhibit the $A\beta_{40}$ fibrillation.

Hsp90 inhibits $A\beta_{40}$ peptide secondary structure transitions during fibrillation

To investigate the influence of Hsp90 proteins on Aβ peptide secondary structure, we carried out CD spectroscopy measurements. CD spectra were recorded over time to quantify the secondary structure transition of the $A\beta_{40}$ peptides with or without the different Hsp90 forms. The aggregation of 10 μM $A\beta_{40}$ in the presence or absence of 0.04 μM Hsp90 was monitored in the far-UV region from 190 to 260 nm after 0, 0.5, 1, 1.5, 2, 3, 4, 5, 6, 7, 8, and 22 h incubation at 37°C. Figure 2 and Figure S1 illustrate that the CD spectrum of $A\beta_{40}$ at time zero is characterized by a typical random coil conformation, with a characteristic minimum at ~198 nm. As the incubation time increases, the random coil conformation of $A\beta_{40}$ converts gradually into the

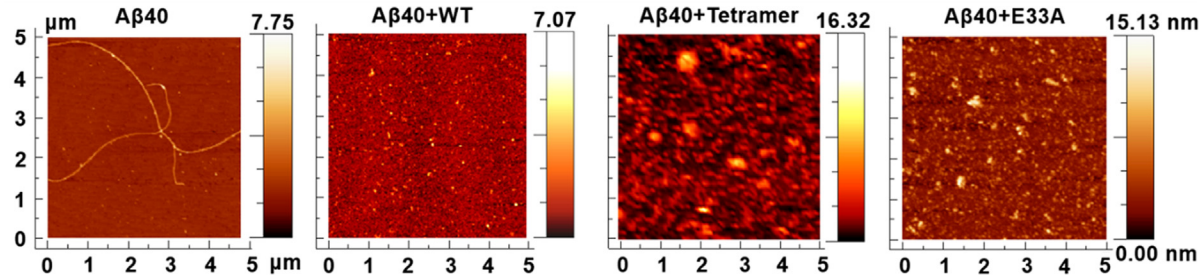

Figure 1. Hsp90 inhibits fibril formation of $A\beta_{40}$. AFM images of 10 μM $A\beta_{40}$ in the presence or absence of 0.5 μM Hsp90 forms (WT, tetramer, or E33A mutant) after incubation at 37°C for 24 h at 300 rpm, show that Hsp90 morphologically inhibits the fibril formation of $A\beta_{40}$. The color scales indicate height values.

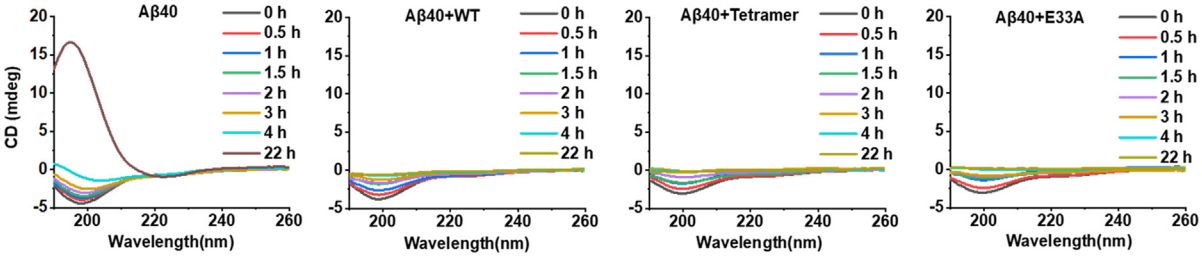

Figure 2. Hsp90 inhibits secondary structure transition of $A\beta_{40}$. CD spectroscopy of 10 μM $A\beta_{40}$ in the presence or absence of 0.04 μM Hsp90 (WT, tetramer, and E33A mutant) after incubation at 37°C and measured immediately after mixing with a pipette, indicates that Hsp90 prevents the secondary structural transition of $A\beta_{40}$ from random coil to β-sheets.

typical β-sheet structure showing the characteristic curve with a minimum at ~220 nm and a maximum at ~195 nm via an isodichroic point at ~210 nm, similar to the result in our previous study.[41] However, in the presence of Hsp90 proteins, no signal corresponding to a β-sheet secondary structure conformation is observed and the signal of the initial $A\beta_{40}$ random coil secondary structure conformation decreases step by step as the incubation carries on and finally disappears. The latter might, to a large extent, be caused by some large aggregates formed by Hsp90 and $A\beta_{40}$. Three Hsp90 forms at a low concentration of 0.04 μM are similarly efficient in inhibiting the secondary structure transition of the $A\beta_{40}$ peptides. Based on our AFM and CD spectroscopy results, we suggest that Hsp90 structurally modulates the transition pathway of $A\beta_{40}$ aggregation and morphologically impedes the formation of $A\beta_{40}$ fibrils.

Hsp90 impedes the secondary pathways of $A\beta_{40}$ fibrillation

By using a ThT kinetics assay, we investigated how $A\beta_{40}$ amyloid fibrillation kinetics is modulated by Hsp90 proteins. ThT is a commonly used fluorescence dye to monitor the formation of amyloid fibrils, as its fluorescence intensity sharply increases when bound to amyloid fibrils.[42] Figure 3 and Figure S2(A) show the results of the ThT kinetic fluorescence assays. In non-agitating condition, all Hsp90 proteins inhibit $A\beta_{40}$ fibrillation in a concentration-dependent manner, with WT being the most efficient, probably because it is more dynamic than the other forms. The general aggregation course of amyloid protein aggregation is shown in Figure 3(A). Calculated from sigmoidal curve fitting, the phenomenological parameters t_{lag} and $t_{1/2}$ of the fibrillation of 10 μM $A\beta_{40}$ alone were estimated to $t_{lag} = 8.6 \pm 1.56$ h and $t_{1/2} = 10.8 \pm 0.95$ h and Hsp90 significantly prolongs the t_{lag} and $t_{1/2}$ of the fibrillation, as the concentration of Hsp90 increases (Figure 3(B) and (C)).

To get further insight into the microscopic mechanisms of $A\beta_{40}$ fibrillation in the presence of Hsp90, global fit analysis of the kinetic data was performed with an integrated rate law[43–46] by using the AmyloFit online software server.[47] It has been reported that amyloid proteins usually aggregate through either primary or secondary dominated pathways[44,48] and $A\beta_{40}$ undergoes fibrillation mainly via secondary nucleation processes.[41,48] Therefore, we selected the secondary nucleation dominated model and first fitted the ThT data of $A\beta_{40}$ alone, obtaining a set of parameters including the primary nucleation rate constant (k_n) = 0.00174 in concentration^{-nc+1} time^{-1} (nc is the reaction order of primary nucleation that simply interpretates

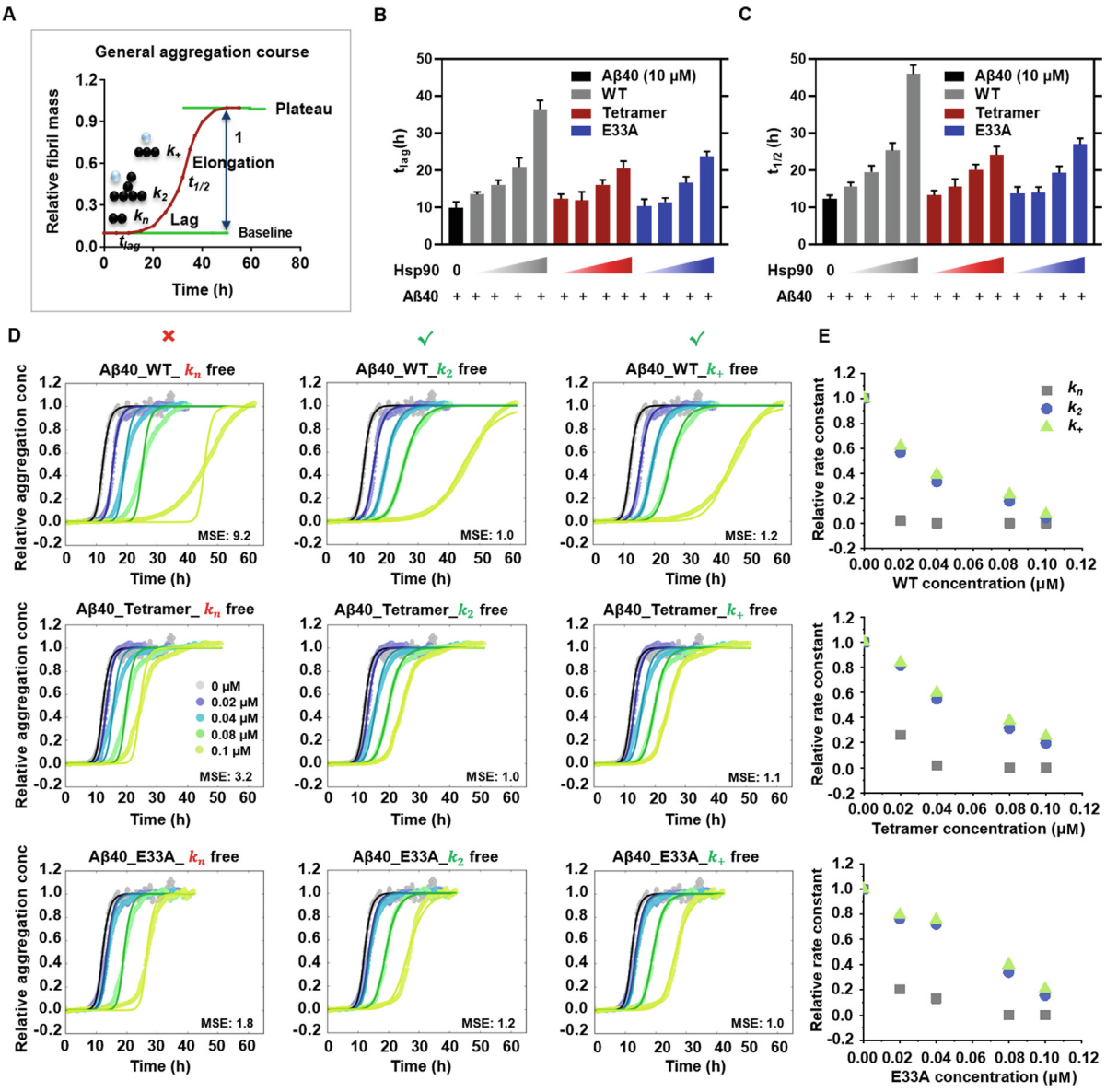

Figure 3. $A\beta_{40}$ aggregation kinetics. (A) General aggregation course of amyloid protein fibrillation. Typically, this process goes through the lag-, elongation-, and plateau- phases, in which primary nucleation (rate constant, k_n), secondary nucleation (rate constant, k_2), and/or elongation (rate constant, k_+) processes are involved. (B) and (C) The t_{lag} and $t_{1/2}$ of the fibrillation of 10 μM $A\beta_{40}$ in the absence or presence of different Hsp90 forms (WT, tetramer, and E33A) at concentrations of 0.02, 0.04, 0.08, and 0.1 μM, were derived from sigmoidal fitting of ThT data of each repeat. Error bars represent standard deviation of at least three replicates (D) Secondary processes of $A\beta_{40}$ fibrillation are influenced by Hsp90. Aggregation kinetics of 10 μM $A\beta_{40}$ in the absence or presence of different Hsp90 forms were monitored by ThT fluorescence over time (the raw data can be found in Figure S2(A)) and then globally fitted by using the *AmyloFit* online software server.[47] For the fitting procedure, the data of $A\beta_{40}$ alone were first fitted (the result is shown in Figure S3) with a secondary nucleation dominated model, from which a set of parameters including k_n = 0.00174 in concentration^{-nc+1} time^{-1}, k_2 = 7.11e^{+7} in concentration^{-n2} time^{-1}, and k_+ = 9.22e^{+6} in concentration^{-1} time^{-1} of $A\beta_{40}$ fibrillation were obtained and used as the initial guess values for the following global fit. Each one of the rate constants k_n, k_2, or k_+ was fitted freely, while the other two were set as initial guess values, by choosing the secondary nucleation dominated model. When k_2 and k_+, but not k_n, were freely fitted then the data was well described (see main text for details). ❖ The mean square error (MSE) values for each set of $A\beta_{40}$ /Hsp90 samples were normalized against the one with the best fit (lowest MSE value). (E) Relative rate constants (relative to the rate constants of $A\beta_{40}$ alone) derived from global fitting for different concentrations of Hsp90.

a nucleus size), the secondary nucleation rate constant (k_2) = 7.11e^{+7} in concentration^{-n2} time^{-1} (n_2 is the reaction order of secondary nucleation that simply interpretates a nucleus size), and the elongation rate constant (k_+) = 9.22e^{+6} in concentration^{-1} time^{-1} of Aβ_{40} fibrillation process, which were used as the initial guess values for the following fit. Each one of the three rate constants (k_n,k_2,$k_\pm$) was fitted freely, while the other two were kept as initial guess values. The result of the global fit analysis is shown in Figure 3(D) and the relative rate constants derived from the global fit are presented in Figure 3 (E). The global fit analysis depicts that if the rate constants k_2 and k_+, rather than the k_n, were freely fitted, the results can describe the Hsp90-dependent aggregation data, suggesting that the secondary pathways (the secondary nucleation and/or elongation processes) of Aβ_{40} aggregation are the ones mostly affected by Hsp90 proteins.

Hsp90 modulates the hydrophobic surface of Aβ_{40} peptides

To determine which microscopic rate constant, k_2 or k_+, of Aβ_{40} is most influenced by Hsp90, we performed seeding experiments of Aβ_{40} peptide fibrillation kinetics in the presence and absence of Hsp90 proteins. Pre-formed Aβ_{40} seeds were added at time zero to the samples with Aβ_{40} monomers and Hsp90 proteins. In the presence of seeds, the primary nucleation processes are nearly negligible compared to the secondary processes. At a high seed concentration, with a concave ThT aggregation kinetic curve, the growth of fibrillary aggregates mainly originates from elongation processes. The results of the seeding assays in Figure 4(A) and Figure S2(B) show the absolute and normalized signal corresponding to the aggregation concentration, respectively. It illustrates that the addition of Aβ_{40} seeds to Aβ_{40} monomers (the Aβ_{40} + seeds curve) significantly speeds up the Aβ_{40} fibrillation, reaching the plateau phase within the time the unseeded Aβ_{40} sample remains in the lag phase. Notably, the seeded kinetic curve shows a concave shape in opposite to the sigmoidal curve for unseeded Aβ_{40}. The unseeded samples with Aβ_{40} supplemented with Hsp90 proteins dramatically slow down the process with slower aggregation kinetics with sigmoidal curves. This is consistent with the results of ThT assay in Figure 3 that all variants inhibit Aβ_{40} fibrillation, with WT being the most efficiently. In both Figures 3(D) and 4(A), the mutant E33A without ATPase activity inhibits Aβ_{40} fibrillation, suggesting that Aβ_{40} may not only bind to one specific site on Hsp90, and that the ATPase activity is also not the only determinant in the effect of Hsp90 on Aβ_{40} fibrillation. In the presence of both Aβ_{40} seeds and Hsp90, the fibrillation process of Aβ_{40} is prolonged as compared to Aβ_{40} alone without seeds. This indicates that the elongation process of Aβ_{40} fibrillation with seeds is significantly inhibited by Hsp90.

As both hydrophobic and electrostatic interactions play an important role in the aggregation process of amyloid proteins,[16] we performed ANS (8-anilino-1-naphthalenesulfonic acid)[49] fluorescence studies (see methods) to understand the effect of Hsp90 protein on the surface hydrophobic reorganization of Aβ_{40} peptides. The ANS assay was conducted for 10 μM Aβ_{40} in the presence or absence of 0.1 μM Hsp90 protein forms, to check how Hsp90 influence the hydrophobic surface and the fibrillation behavior of Aβ_{40} (Figure 4(B)). The decrease of the fluorescence signal after the addition of Hsp90 WT, tetramer or mutant (E33A) compared to that of Aβ_{40} alone, suggests that the hydrophobic surface of Aβ_{40} to interact with ANS is decreased. Among these Hsp90 proteins, Hsp90 WT is the most effective one to reduce the hydrophobic surface of Aβ_{40}, which is in line with our ThT data, with Hsp90 WT as the most effective inhibitor against the fibrillation. This suggests that the accessible hydrophobic surfaces of Aβ have a crucial role in Aβ fibrillation.[15] But if this was the only effect, a red-shift of the emission peak would have been expected. Therefore, some electrostatic interaction will also be involved.[50]

To further investigate the aggregation behavior, a photo-induced crosslinking experiments was carried out to stabilize 90 μM Aβ_{40}, in the absence or presence of 2 μM Hsp90. The data in Figure 4 (C) and (D) suggest that Aβ_{40} alone aggregates into a series of different oligomer sizes, but that Hsp90 significantly retains Aβ_{40} as monomers on the SDS-PAGE gel, with the wild type Hsp90 being the most efficient.

Therefore, we can propose that the Hsp90 slows down the elongation process of Aβ_{40} fibrillation presumably by decreasing the accessible hydrophobic surfaces of Aβ_{40} and thus keeping the peptides as monomers or small oligomers.

To further confirm this observation, we continued with a photo-induced cross-linking assay[51,52] to stabilize Aβ_{40} samples but this time at the end point of the ThT assay (Figure 4(E). Results of reference experiments conducted with samples at 0 h are shown in Figure S4(B), indicating that Hsp90s almost show no effect on Aβ_{40} fibrillation at time zero of ThT experiment). In the presence of Hsp90, Aβ_{40} monomers were observed, while almost no Aβ_{40} monomers were found in the absence of Hsp90 on the SDS-PAGE gel after the cross-linking assay, which might be caused by the formation of the fibrils that are too large to go through the SDS-PAGE gel.

Figure 4(C) also shows some higher-molecular-weight proteins, which probably are Hsp90 aggregates after the cross-linking at a high concentration (2 μM), which is less present at a low concentration (0.5 μM) (Figure 4(E)). In Figure 4(E), the bands above 170 kDa can be

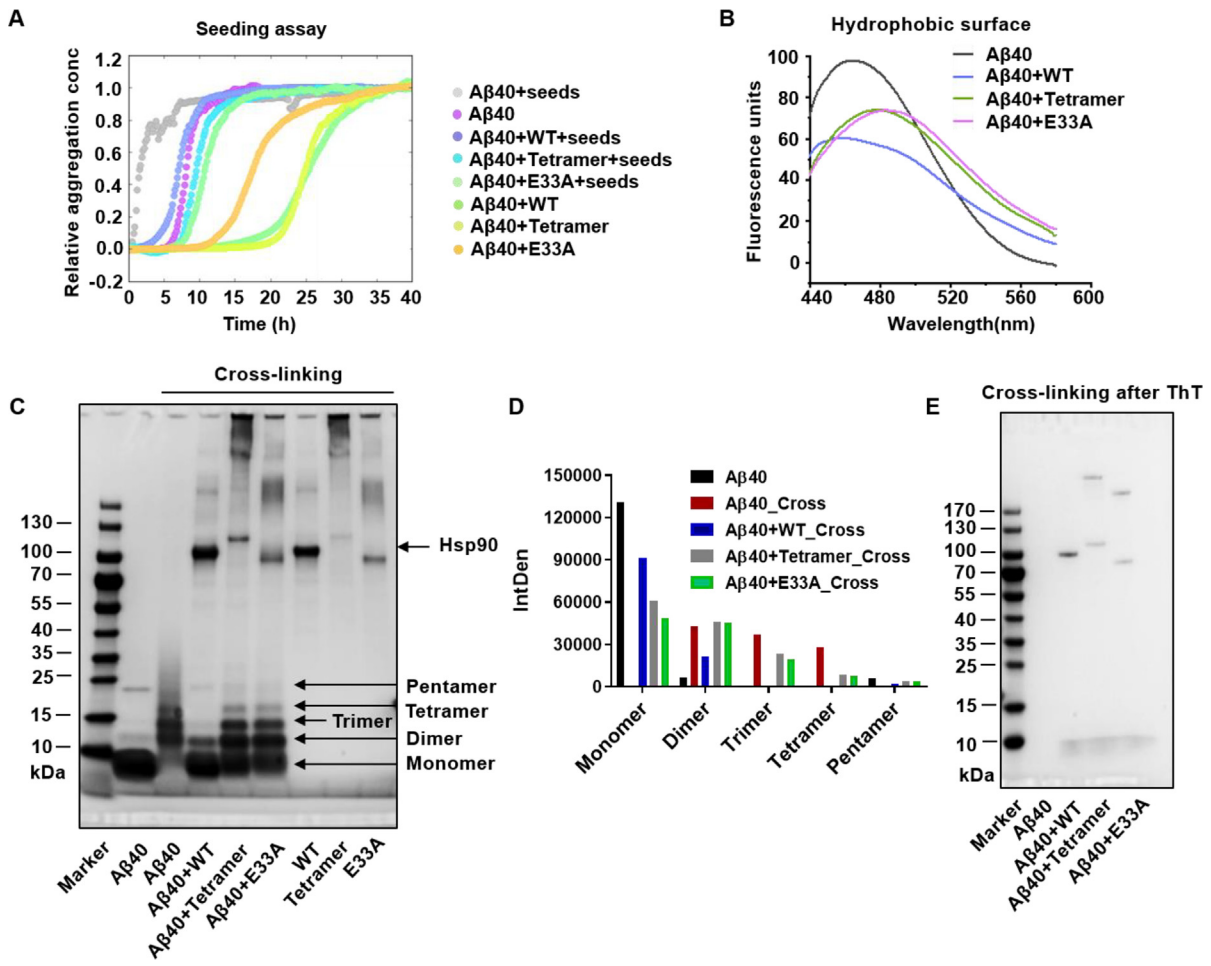

Figure 4. Hsp90 inhibits the elongation process of $A\beta_{40}$ fibrillation by attenuating hydrophobic interactions among the $A\beta_{40}$ peptides. (A) The seeding experiments of 10 μM $A\beta_{40}$ in the presence of 1 μM $A\beta_{40}$ seeds without (gray) or with 0.1 μM Hsp90 protein WT (blue), tetramer (cyan) or mutant E33A (light green), monitored by ThT fluorescence at 37 °C without agitation. As controls, 10 μM $A\beta_{40}$ fibrillation kinetic assays were conducted without the seeds in the absence (purple) or presence of 0.1 μM Hsp90 protein WT (green), tetramer (yellow) or mutant E33A (orange). (B) ANS fluorescence assay performed with 10 μM $A\beta_{40}$ in the presence or absence of 0.1 μM Hsp90 protein variants at 37 °C. (C) SDS-PAGE of the photo-induced cross-linking samples of 90 μM $A\beta_{40}$ in the presence or absence of 2 μM Hsp90 after 15 min incubation at room temperature. (D) Quantitative comparison of oligomers from the cross-linking experiment. (E) SDS-PAGE of the photo-induced cross-linking samples of 10 μM $A\beta_{40}$ with or without 0.5 μM Hsp90 after the ThT assay shown in Figure S4(A).

SDS-resistant wild-type or E33A Hsp90 tetramers and $A\beta_{40}$ fibrils do not run into the page because of the insolubility. 10 μM $A\beta_{40}$ peptides in the presence of 0.5 μM Hsp90 likely remain as monomers before (Figure S4(B)) or after (Figure 4 (E)) the ThT assay, supporting that 0.5 μM Hsp90 WT or variant completely suppresses $A\beta_{40}$ fibrillation in Figure S4(A). These results also show that Hsp90 retains $A\beta_{40}$ as mainly monomeric species and slows down the fibril formation *in vitro*.

ATP modulates the hydrophobic surface of Hsp90 and thereby $A\beta_{40}$ fibrillation

To investigate the potential mechanism by which ATP affects the protective activity of Hsp90 protein against $A\beta_{40}$ fibrillation, we conducted kinetic aggregation studies with 10 μM $A\beta_{40}$ and 0.1 μM Hsp90 (WT) in the absence or presence of 2 mM ATP or AMP-PNP. It is well known that ATP slightly shifts Hsp90 towards a closed conformation and AMP-PNP mainly locks Hsp90 in the closed conformation.[1,53] The aggregation kinetics observed in Figure 5(A) and Figure S2(C) indicate that ATP or AMP-PNP on its own (i.e. in the absence of Hsp90) does not significantly influence $A\beta_{40}$ fibrillation, but that both negatively regulate the effect of Hsp90 on $A\beta_{40}$ fibrillation.

Again, we used the ANS fluorescence assay to test for hydrophobic surfaces, this time of 6 μM Hsp90 (WT) on its own, in the absence or presence of 2 mM ATP or AMP-PNP. Figure 5(B) shows the reduction of the hydrophobic surface of

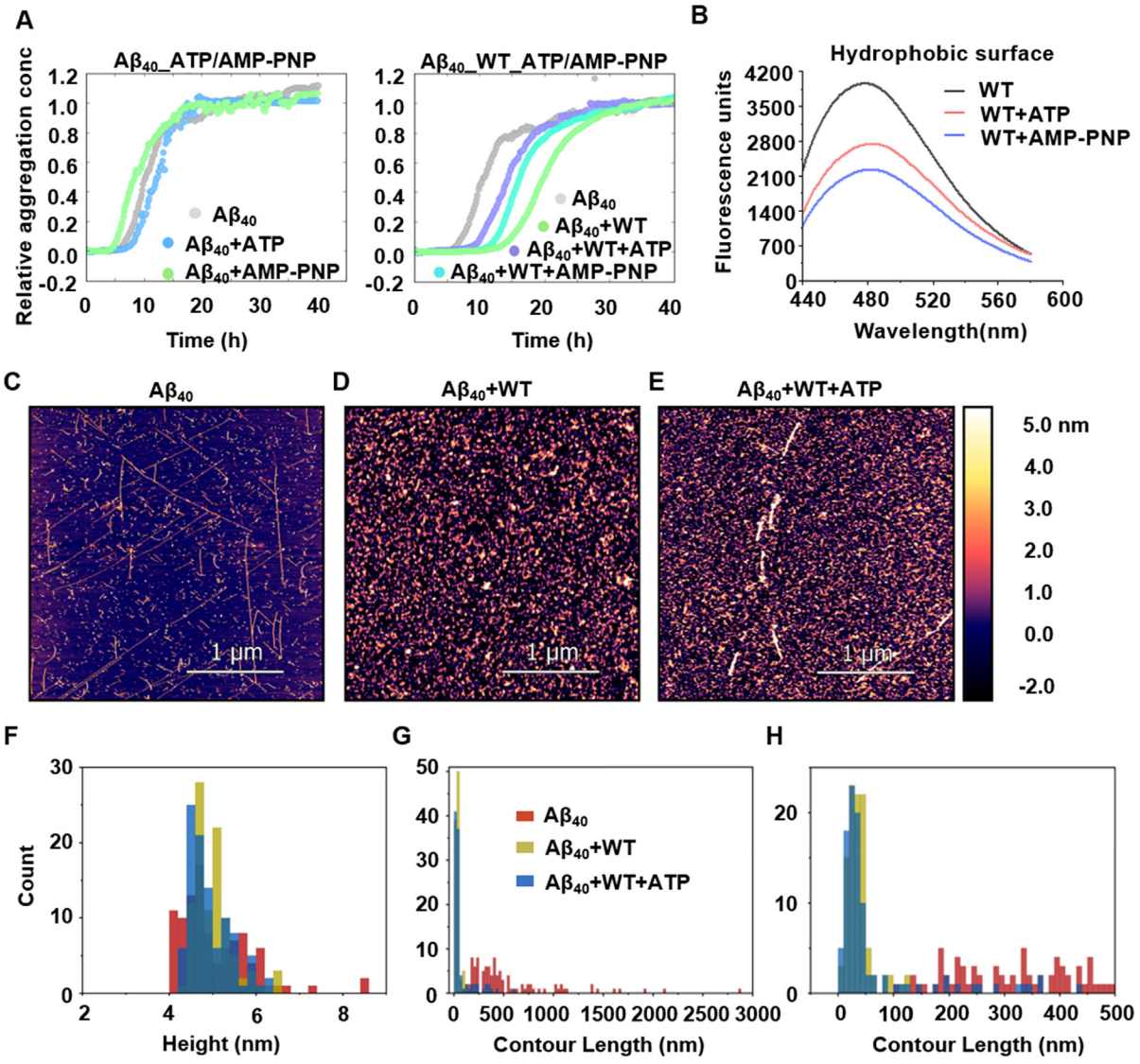

Figure 5. (A and B) ATP negatively regulates the inhibitory efficiency of Hsp90 against Aβ_{40} fibrillation by modulating the conformation dynamics and reducing hydrophobic surfaces of Hsp90. (A) Aggregation kinetics of Aβ_{40} fibrillation monitored by ThT fluorescence. The experiment was conducted with 10 μM Aβ_{40} and 0.1 μM Hsp90, in the presence or absence of 2 mM ATP or AMP-PNP at 37 °C without agitation, and the averaged data were normalized with *AmyloFit*. The normalized data of individual curves were shown in Figure S5. (B) ANS fluorescence experiment performed with 6 μM WT Hsp90 in the presence or absence of 2 mM ATP or AMP-PNP at 37 °C. (C–H) Results of AFM imaging in liquid. (C) Aβ_{40} peptides only. (D) Aβ_{40} peptides with Hsp90 (10:1). (E) Aβ_{40} peptides with Hsp90 (10:1) and ATP (5.0 mM). All samples (Aβ_{40} concentration: 75 μM) were incubated for 92 h at 300 rpm at 30 °C. The respective sample was deposited on a flat mica surface and measured in HEPES pH 7.0 with 10 mM $MgCl_2$ with a scan size of 3 μm × 3 μm and a scan rate of 2.44 Hz. In total, about 5 images of each sample were taken and the experiments were performed twice. (F) Height histograms of Aβ_{40} structures, showing height values of 5 (±1) nm in all cases. (G) Contour length histogram (bin width 28 nm) of the Aβ_{40} structures, showing values of (546 ± 464) nm (Aβ_{40} incubation only), (37 ± 23) nm (Aβ_{40} peptides incubated with Hsp90), (72 ± 106) nm (Aβ_{40} peptides incubated with Hsp90 and ATP). The large error for the latter is due to the bimodal distribution (monomers and oligomers). (H) Zoom into the first part of (G) with a bin width of 10 nm. Please note that longer structures (>100 nm) are only visible in the absence of Hsp90 (red) or if Hsp90 + ATP are present (blue).

Hsp90 upon the addition of the nucleotides, which likely has the negative regulatory inhibition efficiency of Hsp90 against Aβ_{40} fibrillation. Our hydrophobicity assay agrees with the observed fibrillation kinetics: the accessible hydrophobic surface decreases from apo Hsp90 to ATP/Hsp90

to AMP-PNP/Hsp90, similar to the inhibitory effects of Hsp90 on $A\beta_{40}$ fibrillation in Figure 5(A). The decrease of Hsp90 inhibition by AMP-PNP is not as strong as for ATP, indicating that the hydrophobicity is not the only determinant, but that conformational dynamics likely also plays a significant role.

We then further confirm the inhibitory effect of Hsp90 on $A\beta_{40}$ fibrillation and the influence of ATP on this effect by using AFM imaging in aqueous environment under various conditions. First $A\beta_{40}$ was incubated for 92 h at 300 rpm and 30 °C at a concentration of 75 μM to form mature fibrils (Figure 5(C)). The same experiment was repeated in the presence of Hsp90 ($A\beta_{40}$: Hsp90 ratio of 10:1). Figure 5(D) shows that no fibrils were formed, i.e. that Hsp90 efficiently inhibited $A\beta_{40}$ fibrillation at substoichiometric concentrations, consistent with previously reported experiments.[28] Finally, the same experiment was repeated with Hsp90 in the presence of 5 mM ATP. In this case, some fibrils could be observed, but to a much lower extent as with $A\beta_{40}$ alone (Figure 5(E)). Figure 5 (F)–(H) show the heights and contour lengths of $A\beta_{40}$ aggregates under the various conditions. The AFM images show straight and spiral fibrils, with contour lengths around 500 nm, which were formed in the absence of Hsp90 and ATP. The height of the fibrils is around 5 nm in agreement with previous reports.[32,34] In the presence of Hsp90 and absence of ATP, mainly monomers and oligomers with contour lengths below 50 nm were observed representing most likely monomers or small co-aggregates of $A\beta_{40}$ and Hsp90. In the presence of Hsp90 and ATP, monomers, oligomers as well as fibrils were observed, indicating a suppressing effect of ATP on the capability of Hsp90 to inhibit the fibrillation process.

Binding mode between Hsp90 and the $A\beta_{40}$ peptides

To investigate the binding affinity between Hsp90 and Aβ peptides, fluorescence polarization (FP) experiment was carried out. The result shown in Figure 6(A) indicates that Hsp90 does not display any strong affinity (K_d is estimated to be lower than 100 μM) for the $A\beta_{40}$ peptides (monomers) in the absence or presence of AMP-PNP. Both closed and open Hsp90 proteins presumably protect the $A\beta_{40}$ peptides from the fibrillation via surface hydrophobic solubilization rather than a specific interaction, in agreement with our ANS assays where Hsp90 stabilizes Aβ with changed hydrophobic surface. As shown in Figure S6, Hsp90 with open conformation offers more hydrophobic surfaces than that in closed state, supporting Figure 5(A) and (B) where Hsp90 without AMP-PNP has more hydrophobic surfaces and better inhibition efficiency than the one with

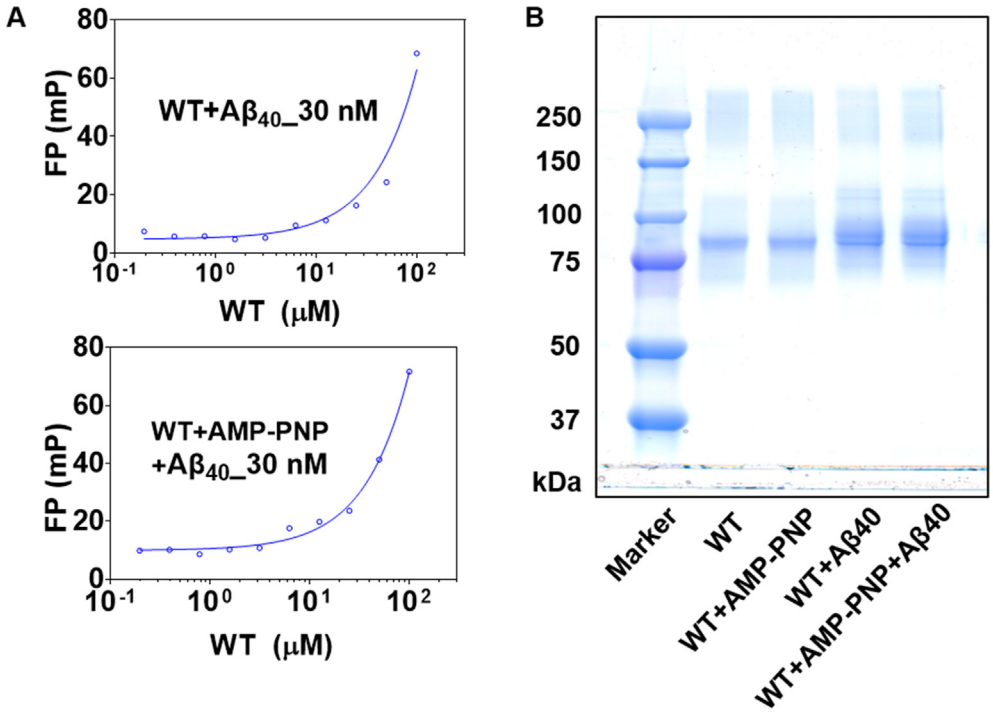

Figure 6. (A) Fluorescence polarization (FP) assays conducted with 30 nM HL488-$A\beta_{40}$ and Hsp90 (WT, 0–100 μM, two-fold serial dilution) in the absence or presence of AMP-PNP. (B) SDS-PAGE of the photo-induced cross-linking samples of 2 μM Hsp90 (WT) and 90 μM $A\beta_{40}$ with or without AMP-PNP after 15 min incubation at room temperature. Hsp90 and $A\beta_{40}$ form complexes in the presence or absence of 2 mM AMP-PNP.

AMP-PNP (closed state). The weak/unspecific interaction between Hsp90 and $A\beta_{40}$ can be converted to covalent connection through PICUP.[54] To further investigate if Hsp90 offers the surfaces for Aβ solubilization, the PICUP experiments were conducted (Figure 6(B)), followed by the LC/MS analysis in Figure S7(A) and (B). Hsp90 forms more higher-molecular-weight bands in the presence of $A\beta_{40}$ on the SDS-page gel than these without $A\beta_{40}$ in Figure 6(B), suggesting that Hsp90 forms several complexes with different numbers of $A\beta_{40}$ monomers. Followed by liquid chromatography, ESI–time-of-flight (TOF) mass spectrometry enables to determine the spectrum m/z of the Hsp90 complexes from the PICUP assay. As shown in Figure S7(A), PICUP products eluted from the column with different elution times indicate the formation of Hsp90 complexes with different polarities. Hsp90 without PICUP gives a single peak in the m/z spectra in Figure S7(B). After PICUP, Hsp90 with the $A\beta_{40}$ peptides (in green and red curve, Figure S7(B)) seems to form more complexes in comparison to the one without the peptides (in purple curve, Figure S7(B)). Altogether this data indicates that Hsp90 solubilizes Aβ peptides to large degree through hydrophobic surfaces as suggested by the ANS assay, although the binding to monomers is weak, which we conclude from our fluorescence polarization assay. This is consistent with the interaction of Hsp90 with several disordered proteins like tau via a transient and weak binding on the extended substrate binding surfaces that crosses the domain boundaries.[14]

Discussion

Here we report how wild type Hsp90 and Hsp90 variants slow down $A\beta_{40}$ peptide fibril formation at substoichiometric ratios *in vitro*. Our AFM and CD experiments further show that Hsp90 proteins alter the conversion of secondary structure conformations of $A\beta_{40}$ during fibrillation and induce formation of amorphous $A\beta_{40}$ aggregates. Our global fit analysis of the kinetic data suggests that Hsp90 proteins influence both the secondary nucleation and elongation processes. The seeding assay confirms the finding that the elongation process of $A\beta_{40}$ is significantly modulated by Hsp90. The cross-linking assay further shows that, in the presence of Hsp90, $A\beta_{40}$ even remains predominantly in its monomeric state compared to in the absence of Hsp90 proteins. In order to elucidate the molecular mechanisms behind the interaction between Hsp90 and $A\beta_{40}$, an ANS fluorescence assay was conducted, from which we conclude that Hsp90 decreases the accessible hydrophobic surfaces of the $A\beta_{40}$ peptides.

The Hsp90 protein is intrinsically flexible with a number of accessible hydrophobic surfaces[55] and coexists in various conformations. Furthermore, the conformational transition of Hsp90 can be modulated upon the binding of diverse substrates, co-chaperones, adaptor proteins, or nucleotides.[10,56–59] Here we investigated the effect of nucleotides by repeating the experiments in the presence of ATP or the non-hydrolysable AMP-PNP. In particular, our ThT kinetics experiments show that ATP alone hardly inhibits the aggregation of $A\beta_{40}$, which is consistent with a previous study.[60] On the contrary, the inhibitory effect of Hsp90 on $A\beta_{40}$ fibrillation is significantly attenuated by the addition of ATP, while AMP-PNP reduces this effect of Hsp90 to a lower extent, confirming that our observations are related to the conformational dynamics of Hsp90 proteins. To study the influence of ATP on the hydrophobicity and electrostatic interactions of Hsp90, an ANS fluorescence assay was conducted, which shows that ATP or AMP-PNP decreases the total hydrophobic surface of Hsp90. Thus, ATP diminishes the inhibitory effect of Hsp90 on $A\beta_{40}$ fibrillation also by decreasing the hydrophobic surface of Hsp90. Nevertheless, this is likely not the only effect, as ATP reduces the inhibitory effect of Hsp90 more than AMP-PNP, despite AMP-PNP having a larger effect on the hydrophobic surface (Figure 5(A) and (B)). Therefore, we speculate that also the large conformational dynamics of Hsp90s plays a crucial role. In addition, ATP hydrolysis might displace $A\beta_{40}$ monomers from Hsp90, further reducing the inhibitory potency of Hsp90.

We briefly summarize in a schematic model in Figure 7 how $A\beta_{40}$ fibrillation can be influenced by Hsp90 as well as ATP at the microscopic and molecular levels: (1) Hsp90 inhibits the fibrillation (mostly the elongation process) of $A\beta_{40}$ monomers by interfering with the hydrophobic interactions between $A\beta_{40}$ monomers and/or oligomers; (2) ATP suppresses the inhibitory effect of Hsp90 on $A\beta_{40}$ fibrillation. Conceivably, ATP triggers a conformational conversion of Hsp90's quaternary structure even in the presence of $A\beta_{40}$ and thus reduces the global hydrophobic surfaces of Hsp90, leading to the release of the Hsp90-bound $A\beta_{40}$ peptides and/or less binding of free $A\beta_{40}$. In other words, ATP hydrolysis would lead to something considered as a 'clean cycle' to leave the relatively bare Hsp90 and more unbound $A\beta_{40}$ available for fibrillation. AMP-PNP on the other hand is known to close the Hsp90 dimer and therefore stably reduce the accessible hydrophobic surface of Hsp90. This is consistent with the concept that Hsp90 usually interacts with its clients via a large number of low energy contacts in a dynamic and transient way.[61] Similar to the hydrophobic surfaces of Hsp90 for $A\beta_{40}$, the binding site of Tau on the Hsp90 mainly consists of hydrophobic residues.[10] The binding surface of $A\beta_{40}$ or Tau[10] on Hsp90 are generally in accordance with how Hsp90 interacts with the other amyloid proteins, like the misfolded transthyretin monomer,[62] the GR-LBD (glucocorticoid receptor-ligand binding domain),[57] or the unfolded kinase

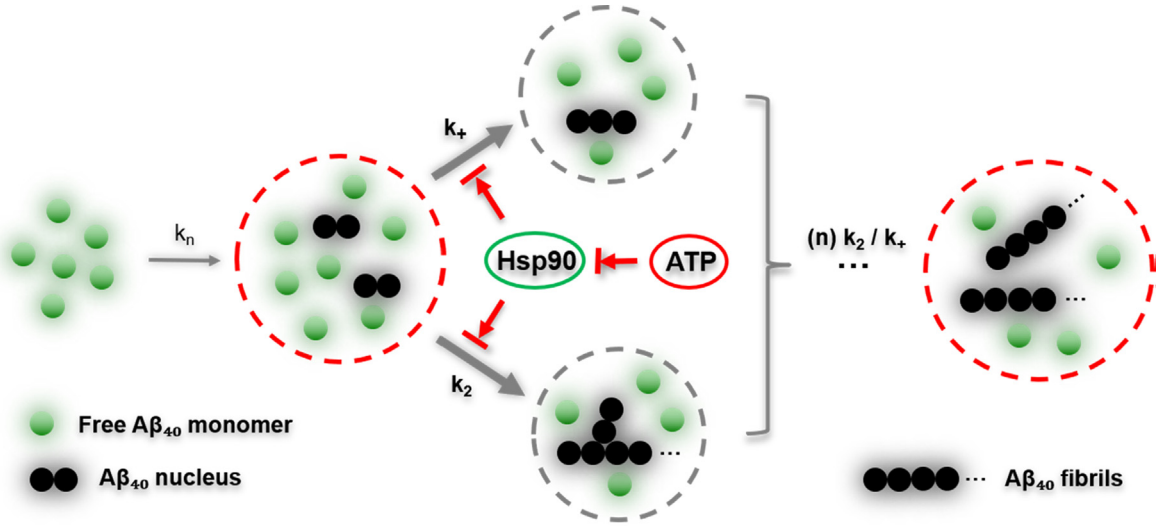

Figure 7. Schematic diagram of the inhibitory effect of Hsp90 on $A\beta_{40}$ fibrillation in the presence and absence of ATP. The fibrillation of $A\beta_{40}$ peptides occur via primary nucleation, elongation and secondary nucleation mechanisms, here described as the rate constants, k_n, k_+, and k_2. Secondary nucleation is the dominating process for an increase of aggregate mass during $A\beta_{40}$ amyloid formation, after which the pre-fibrils undergo several (n) elongation/secondary nucleation processes, to become mature fibrils. The presence of Hsp90 provides exposed hydrophobic surfaces to which various $A\beta_{40}$ species can bind, leading to a decrease of free $A\beta_{40}$ monomers and/or oligomers that are available to form new nuclei and for the subsequent elongation and secondary nucleation processes. ATP modulates the global conformation and surface hydrophobicity of Hsp90, and therefore reduces the activity of Hsp90 against, mostly, the elongation process of $A\beta_{40}$ fibrillation.

Cdk4.[63] Since $A\beta_{40}$ is 10 times size smaller than Tau, Hsp90 may stoichiometrically bind to more $A\beta_{40}$ compared to Tau or other amyloid protein. Tau takes 106-Å-long binding patch of Hsp90 for the low-affinity interaction,[10] while Hsp90 forms several complexes with different numbers of $A\beta_{40}$ monomers as observed by the PICUP in Figure 6 (B) and the following LC-MS assay (Figure S7(A) and (B)) with low binding affinity (Figure 6(A)).

We still do not fully understand the molecular action of the tetramer and E33A mutant, as shown in Figure 4(A) and (B), because the tetramer and E33A show similar effects regarding the reduction of $A\beta_{40}$ hydrophobicity but a different effect of $A\beta_{40}$ fibrillation. Nevertheless, the tetramer and E33A helped us to delineate factors that determine the interaction between Hsp90 and $A\beta_{40}$. It became clear, that the ATPase activity is very important, but not the only determinant. One other determinant is a reduction of Hsp90 hydrophobicity. Besides, we are convinced that a third determinant is the conformational dynamics/flexibility of Hsp90, but this is a point of further investigation.

Taken together, the different behaviors of $A\beta_{40}$ fibrillation in the presence of wild type Hsp90 and the variants are presumably caused by Hsp90 conformation dynamics, ATPase activity, hydrophobicity, and the heterogeneity of $A\beta_{40}$ aggregation process. This can also explain the differences in the behavior of $A\beta_{40}$ aggregation kinetics in the presence of different Hsp90 isoforms in Figures 3(D) and 4(A). Like other oligomeric proteins[64], tetrameric Hsp90 may equilibrate to dimer or monomer. The equilibria might cause the interface change[65] of tetrameric Hsp90, therefore changing the different hydrophobic surfaces for $A\beta_{40}$ and leading to the similar effect with that of E33A mutant. The tetrameric equilibria and $A\beta_{40}$ aggregation can be further explored but are not an aim of our study. Oligomer equilibria can be dependent of sample preparation conditions, like temperature. The different equilibrium of Hsp90 tetramer may explain the slight different effects of the tetramer on $A\beta_{40}$ fibrillation shown in Figures 3(D) and 4(A).

On the physiological relevance, we can only speculate. In Alzheimer's disease, mitochondrial electron transport chain is severely affected by Aβ aggregation, leading to a decrease of ATP production.[66] With less ATP, there might be less Hsp90-client complexes. Instead, there could be more accessible hydrophobic surfaces on client-free Hsp90 available for binding Aβ, inhibiting the aggregation, and further restoring the function of ATP production. Although the direct physiological relevance of Hsp90 and ATP for modulating Aβ fibrillation remain to be explored, increasing evidence indicates that Aβ can be produced and can aggregate inside cells and that there is a communication between the extracellular and intracellular Aβ pools.[67–70] Furthermore, our study provides a

potential mechanism how Hsp90 and variants may regulate Aβ fibrillation. These shed light on the multiple facets of the chaperone Hsp90 interaction with amyloid proteins.

Materials and Methods

Purification of recombinant Hsp90 from *E. Coli*

Gene expression and subsequent protein purification was performed following established protocols with minor modification.[71] The construct used in this study were yeast Hsp90 WT carrying an N-terminal His_6-*tag* and yeast Hsp90 E33A with a substituted charged linker region and a cleavable His_6-SUMO-*tag*.[1] In short, pET28 derived expression constructs were transformed with BL21 Star (DE3) cells. Gene expression was induced at OD_{600} = 0.7 with 1 mM IPTG in cells grown in *lysogeny broth* media at 37 °C. The cells were harvested 4 h after induction.

Cells were resuspended in HEPES buffer 'pH7.5' containing 150 mM NaCl and 20 mM Imidazole and lysed with a Cell Disrupter (Constant Systems) at 1.6 kbar. Cleared lysate was then applied to HisTrap HP column followed by anion exchange chromatography with HiTrap Q and gel filtration on S200 (all columns GE Healthcare). Fractions corresponding to the dimer and to a higher oligomer were pooled separately. The protein was flash frozen in liquid nitrogen in concentrations of 130–315 μM and stored at −80 °C. Cleavage of the SUMO-*tag* was done by dialysis of the HisTrap eluate in the presence of 1/100 mol SENP protease against imidazole free buffer and removal of free SUMO and uncleaved fusion-protein by a second HisTrap.

The oligomeric state of the higher oligomer was examined with right angle light scattering and refractive index analysis (Viscotek TDA 305) after separation on a S200 10/300 GL increase column (GE Healthcare) confirming a predominantly tetrameric composition.

Other materials and sample preparation

Concentrated Hsp90 protein stock solutions were diluted to working concentration in 40 mM Hepes buffer supplemented with 150 mM KCl, pH 7.5. $A\beta_{40}$ was purchased from (Alexo Tech) and Adenosine 5′-triphosphate disodium salt hydrate (ATP, CAS: 34369-07-8), Adenylyl-imidodiphosphate (AMP-PNP, CAS: 25612-73-1), 8-Anilino-1-naphthalenesulfonic acid (ANS, CAS: 82-76-8), Thioflavin T (ThT, CAS: 2390-54-7), Tris (2,2′-bipyridyl) dichlororuthenium(II) hexahydrate (Ru(Bpy), CAS: 50525-27-4), and Ammonium persulfate (APS, CAS: 7727-54-0) were purchased from Sigma-Aldrich. $A\beta_{40}$ stock solutions were prepared by dissolving the lyophilized powder in 10 mM NaOH to a concentration of 2 mg/mL and then sonicated in an ice-water bath for 1 min, as described previously in our publications[75,76]. ATP and AMP-PNP stock solutions were prepared at a concentration of 100 mM in 50 mM Tris-HCL, pH 7.5. ThT and ANS stocks were prepared to 3 and 10 mM in 50 mM Tris buffer pH 7.4 and DMSO, respectively. The concentrations of Ru(Bpy) and APS were 1 and 20 mM in 10 mM sodium phosphate buffer, pH 7.4, respectively. All of the buffers, 10 mM NaOH, ThT and ANS stocks were filtered with 0.2 μm (micrometer) syringe-driven filters.

ThT fluorescence assays

To study the effect of Hsp90 (WT, tetramer, and E33A mutant) on the fibrillation kinetics of the $A\beta_{40}$ peptides, Hsp90 solutions at the different concentrations (0, 0.02, 0.04, 0.08, and 0.1 uM) were prepared with 40 μM ThT and 10 μM $A\beta_{40}$ in the assay buffer (20 mM sodium phosphate buffer, pH 7.4, 0.2 mM EDTA, 0.02% NaN_3) on ice. 40 μL of each sample was then transferred into a 384-well black plate with transparent bottom (NUNC) and sealed with a piece of foil film. The plate was incubated in a microplate reader (PHERAstar FSX, BMG LABTECH, Germany) and the fluorescence kinetics of $A\beta_{40}$ was monitored at 37 °C without agitation every 5 min, using wavelengths of 430 nm and 480 nm for excitation and emission, respectively.

To investigate how ATP and AMP-PNP affect the activity of Hsp90 on $A\beta_{40}$ fibril formation, we conducted another ThT assay with 40 μM ThT, 10 μM $A\beta_{40}$, 0.1 μM Hsp90 (WT, tetramer, or E33A mutant), in the presence or absence of 2 mM ATP and AMP-PNP. The samples were prepared and the kinetics was monitored in the same way as mentioned above. As a control, the effect of ATP and AMP-PNP on $A\beta_{40}$ fibrillation kinetics was studied as well.

In a seeding assay, 10 μM $A\beta_{40}$ seeds were freshly prepared from a monomeric solution allowed to incubate for ~15 h at 37 °C in a 384-well black plate (NUNC) without agitation. The seeds were then sonicated in ice-water bath for 2 min. The samples were prepared as described above in the presence of 1 μM $A\beta_{40}$ seeds. These ThT assays were conducted with at least three replicates.

All of the original ThT data were plotted with Prism7.0 (GraphPad Software). The averaged ThT data were normalized with equation (1) and globally fitted in AmyloFit,[47] the sigmodial fitting were performed with data of individual curves by using equation (2). The averaged data of seeding assays and the data of individual curves obtained from ThT assays with ATP or AMP-PNP were normalized with equation (1) in *AmyloFit*.

$$y_{norm,i} = (1 - M_{0,frac})\frac{y_i - y_{baseline}}{y_{plateau} - y_{baseline}} + M_{0,frac} \quad (1)$$

$$y = \frac{y_{baseline} - y_{plateau}}{1 + e^{(t-t_0)/dt}} + y_{plateau} \quad (2)$$

where $y_{baseline}$ and $y_{plateau}$ are the values of the data at the baseline and the plateau, $M_{0,frac}$ is the relative initial concentration of aggregates (i.e., a value between 0 and 1). t is the time of amyloid aggregation course and t_0 is the time when the fluorescence intensity reaches half of the plateau value, while dt is the time constant. $y_{norm,i}$ is the normalized value of y_i, the original value of the ith data point, and y was the fitted value of the data at time t. The lag time t_{lag} and aggregation half time $t_{1/2}$ were given as follows.

$$t_{1/2} = t_0 \quad (3)$$

$$t_{lag} = t_{1/2} - 2dt \quad (4)$$

The normalized data, t_{lag} and $t_{1/2}$ were plotted with Prism7.0 (GraphPad software).

Global fitting

To identify which microscopic rate processes of $A\beta_{40}$ aggregation are the ones most influenced by Hsp90, the ThT data of $A\beta_{40}$/Hsp90 (0, 0.02, 0.04, 0.08, and 0.1 μM) were fitted globally with an integrated rate law[43,44] in *AmyloFit* online software server.[47] The secondary nucleation dominated model was selected, the data of $A\beta_{40}$ alone was first fitted, obtaining a set of parameters, which were used as the initial guess values for the following fits. Among these obtained parameters, the primary nucleation rate constant (k_n, with units of time^{-1}-concentration^{-nc+1}, where n_c is the reaction order of primary nucleation that simply interpretates a nucleus size), the secondary nucleation rate constant (k_2, with units of time^{-1}concentration^{-n2}, where n_2 is the reaction order of secondary nucleation that simply interpretates a nucleus size), or the elongation rate constant (k_+, with units of of time^{-1}concentration^{-1}) was fitted freely while the other two rate constants were set as fixed initial values. For detailed definitions of these parameters and fitting procedure, please refer to the nature protocol.[47]

Atomic force microscopy (AFM) imaging in air

For AFM measurement in air, 10 μM $A\beta_{40}$, with or without 0.5 μM Hsp90 (WT, tetramer, or E33A mutant) were incubated at 37 °C in 1.5 mL microcentrifuge tubes for 24 h at 300 rpm. 15 μL of each sample was then added onto the freshly cleaved muscovite mica (Electron Microscopy Sciences) and incubated for 5 min at room temperature. The excess sample was removed with filter paper and the mica plate with the sample was rinsed once with 150 μL of Milli-Q water. The excess water was removed with filter paper and the mica plate with the sample was dried under nitrogen gas. The images were obtained with the Bruker Dimension Icon Scanning Station (Bruker, USA) in intermittent contact mode in air and processed with the WSxM 4.0 software.[72]

Atomic force microscope imaging in liquid

For AFM imaging, $A\beta_{40}$ peptides were diluted with PBS buffer (Dulbecco's Phosphate Buffered Saline, pH 7.2, 500 mL, Sigma-Aldrich, USA) to a final concentration of 75 μM with 7.5 μM Hsp90 (WT), 5.0 mM ATP or 7.5 μM BSA. The peptides were incubated at 30 °C for 92 h at 300 rpm (Eppendorf Thermotop, Germany). A flat mice surface (muscovite, diameter 10–12 mm, Plano, Germany) was cleaved, immobilized on an AFM specimen (diameter: 15 mm) using UV curable glue (NOA 63, Norland Products, USA) and washed with ultrapure water (30 μL, 18.2 MΩ cm, Purelab Chorus 1, Elga LabWater, Germany) and the $A\beta_{40}$ solution was incubated on the mica surface at 60 °C for 30 min. Finally, the surface was washed with ultrapure water (30 μL).

AFM imaging was performed on a Cypher ES (Asylum Research, an Oxford Instruments Company, USA) using a heating/cooling sample stage set to 25 °C and AC mode based on the blueDrive (photothermal excitation). The measurements were performed in HEPES buffer (pH 7.0) with 10 mM $MgCl_2$. The images were obtained with the BioLever-AC40TS cantilevers (Olympus, Japan) with a resonance frequency of about 20–25 kHz in liquid. The following parameters were chosen for the measurements: a scan size of 5 μm, a scan rate of 2.44 Hz, a setpoint of 300–400 mV and a scan angle of 0°.

The images were processed with the Gwyddion Free SPM analysis software (Petr Klapetek, version 2.53).[73] To correct the recorded height image (using the trace image), the data was levelled by mean plane subtraction, the rows were aligned to the median value and the minimum data value was shifted to 0.

Grain analysis using Gwyddion Free SPM analysis software was performed to obtain height values of the imaged structures. First, the threshold of grain-like features was marked. Then, the generated grain data was exported and the height values of the grains were taken to provide histograms, mean and error values using Origin (Version 2019, OriginLab, USA).

The contour length of the structures was determined by Easyworm 1.[74] The respective AFM images were loaded into the software and 100 individual chains were marked using cursors. Then, Easyworm 2 was used to generate the contour length values for each individual chain marked in Easyworm 1 and the raw data was exported to provide histograms, mean and error values using Origin.

Circular dichroism (CD) spectroscopy

In CD spectroscopy, the sample was performed with 10 μM $A\beta_{40}$ supplemented with or without 0.04 μM Hsp90 proteins (WT, tetramer, or E33A

mutant) in 20 mM potassium phosphate buffer, pH 7.0. The CD spectra were recorded in the far-UV region from 190 to 260 nm with a Chirascan plus CD spectrometer (Applied Photophysics Limited, U.K.). The samples were measured in a quartz cuvette with a pathlength of 10 mm at 37 °C immediately after stirred manually with a pipette, using a step size of 1.0 nm, a bandwidth of 1.0 nm, and a time per point of 0.5 s. The spectra were recorded at 0, 0.5, 1, 1.5, 2, 3, 4, 5, 6, 7, 8, and 22 h. The curves were replotted and smoothed by 20 times with the Origin (Version 2018, OriginLab, USA).

Photo-induced cross-linking of unmodified proteins (PICUP)

In the PICUP experiment, 18 μl of 90 μM $A\beta_{40}$ with or without 2 μM Hsp90 (WT, tetramer, or E33A mutant) in 10 mM sodium phosphate buffer, pH7.4, were incubated for 15 min at room temperature, followed by the addition of 1 μL of 1 mM Ru(Bpy) and 1 μL of 20 mM APS, obtaining a reaction volume of 20 μL in PCR tubes. The samples were then irradiated for 2 s and quenched by the addition of 2 μl of 0.5 M 1,4-Dithiothreitol (DTT). These cross-linked samples, together with the 90 μM unlinked $A\beta_{40}$, were subjected to the SDS-PAGE with a 4–20% gel and imaged with the Amersham Imager 600 (GE Healthcare Life Sciences, US). The bands corresponding to $A\beta_{40}$ monomers and different kinds of oligomers were quantified and plotted with ImageJ and Prism 7.0 (GraphPad software), respectively.

The same experiments were carried out for 10 μM $A\beta_{40}$ in the presence or absence of 0.5 μM Hsp90 proteins (WT, tetramer, or E33A mutant) after the ThT kinetics experiments in Figure S4(A), as well as for control samples (at time zero of $A\beta_{40}$ aggregation kinetics), the results of which are shown in Figure S4(B).

The similar experiment was also carried out for 2 μM Hsp90 and 90 μM $A\beta_{40}$ in the absence or presence of 2 mM AMP-PNP with irradiation time of 5 s. The cross-linked samples were then subjected to the SDS-PAGE with a 4–20% gel and imaged with the EPSON Scanner.

LC-MS experiemnts

To check how Hsp90 interacts with $A\beta_{40}$ and how conformation dynamics will influence this interaction, Liquid chromatography-mass spectrometry (LC-MS) experiments were performed with 10 μM Hsp90 in native state, 2 μM Hsp90/2 mM AMP-PNP (cross-linked), 2 μM Hsp90/90 μM $A\beta_{40}$ (cross-linked), and 2 μM Hsp90/2 mM AMP-PNP /90 μM $A\beta_{40}$ (cross-linked). LC/MS analysis was performed on a LCT Premier mass spectrometer and HPLC Waters 2795 (Waters, US). Samples were chromatographed on a Reprosil-PUR 2000 C18-AQ column (3 μm, 100mmX2mm) heated to 50 °C using the following condition (see Table 1):

Fluorescence polarization (FP) assay

To investigate the binding affinity of Hsp90 with $A\beta_{40}$. FP assays were performed with Hsp90 (WT, two-fold serial dilution, with a highest concentration of 100 μM, the results are shown in Figure 6(A)) and 30 nM HL488-$A\beta_{40}$ in the absence or presence of 2 mM AMP-PNP with 480 nm and 520 nm as the excitation and emission wavelengths, respectively. The measurements were performed with a microplate reader (PHERAstar FSX, BMG LABTECH, Germany) at 37 °C. The data were plotted with Prism7.0 (GraphPad software). To confirm these results, we performed the experiments once more with WT at the highest concentration of 160 μM with the same method, and obtained similar results (data not shown).

ANS experiments

To study the effect of ATP and AMP-PNP on the hydrophobic surface of the Hsp90 proteins, the samples were prepared in the presence or absence of 6 μM WT Hsp90 with 2 mM ATP or AMP-PNP and then incubated for 1 h at room temperature. ANS fluorescence dye was added to the prepared samples at a final concentration of 30 μM. ANS is believed to binding to (buried) hydrophobic sites of proteins. The observed features of ANS, a blue shift of fluorescence emission maxima and the increase of fluorescence intensity and lifetime, are generally attributed to the hydrophobicity of a binding site and the restricted mobility of ANS. 40 μL of each mixed sample was then transferred into a 384-well white plate (PerkinElmer, USA). The samples were measured using a multi-mode microplate reader from BioTek at 37 °C, with an excitation wavelength of 400 nm and an emission

Table 1 HPLC Method description

Time (min)	Solvent A (acetonitrile with 0.1% formic acid)	Solvent B (water with 0.1 % formic acid)	Flow (mL/min)
0	2%	98%	0.5
2	25%	75%	0.5
25	50%	50%	0.5
30	80%	20%	0.5

The result of MS experiment was given as the spectrum m/z.

wavelength region of 440–580 nm. The obtained values were averaged, plotted and smoothed with Origin (Version 2018, OriginLab).

We also conducted the ANS experiment to investigate whether Hsp90 (WT, tetamer, and E33A) influence the hydrophobic surface of $A\beta_{40}$. Samples containing 10 μM $A\beta_{40}$ in the presence of 0.1 μM Hsp90 (WT, tetamer, or E33A) were prepared, incubated, and measured in the same way as mentioned above.

CRediT authorship contribution statement

Hongzhi Wang: Conceptualization, Investigation, Validation, Project administration. **Max Lallemang:** Investigation, Validation. **Bianca Hermann:** Investigation. **Cecilia Wallin:** Validation. **Rolf Loch:** Validation. **Alain Blanc:** Investigation. **Bizan N. Balzer:** Conceptualization, Validation. **Thorsten Hugel:** Conceptualization, Validation. **Jinghui Luo:** Conceptualization, Validation, Project administration.

Acknowledgment

We appreciate Natacha Olieric for her kind help with the CD experiment and acknowledge the use of the PSI SPM Userlab at PSI.

Funding

M.L., B.N.B. and T.H. were funded by the Deutsche Forschungsgemeinschaft (DFG, German Research Foundation) under Germany's Excellence Strategy – EXC-2193/1 – 390951807. H.W. was sponsored by the State Scholarship Fund (China Scholarship Council (CSC): 201806200097) and J.L. was supported by the Brightfocus foundation (A20201759S) and Swiss National Science Foundation (310030_197626).

Declaration of Competing Interest

The authors declare that they have no known competing financial interests or personal relationships that could have appeared to influence the work reported in this paper.

Appendix A. Supplementary material

Supplementary data to this article can be found online at https://doi.org/10.1016/j.jmb.2020.11.016.

Received 7 June 2020;
Accepted 11 November 2020;
Available online 19 November 2020

Keywords:
Hsp90;
$A\beta_{40}$;
fibrillation;
conformation;
hydrophobic interaction

Abbreviations:
Hsp90, heat shock protein 90; **ATP**, adenosine triphosphate; **AFM**, atomic force microscopy; **CD**, circular dichroism; **ThT**, Thioflavin T; **ANS**, 8-anilino-1-naphthalenesulfonic acid; **Aβ**, amyloid-β; WT, wild type Hsp90; **GR-LBD**, glucocorticoid receptor-ligand binding domain; **ETC**, mitochondrial electron transport chain; **UPR**, unfolded protein response; **PICUP**, photo-induced cross-linking of unmodified proteins; **ER**, endoplasmic reticulum; **AMP-PNP**, Adenylyl-imidodiphosphate; **APS**, Ammonium persulfate

References

1. Ali, M.M., Roe, S.M., Vaughan, C.K., Meyer, P., Panaretou, B., Piper, P.W., et al., (2006). Crystal structure of an Hsp90-nucleotide-p23/Sba1 closed chaperone complex. *Nature*, **440**, 1013–1017.
2. Huh, W.K., Falvo, J.V., Gerke, L.C., Carroll, A.S., Howson, R.W., Weissman, J.S., et al., (2003). Global analysis of protein localization in budding yeast. *Nature*, **425**, 686–691.
3. Didelot, C., Lanneau, D., Brunet, M., Bouchot, A., Cartier, J., Jacquel, A., et al., (2008). Interaction of heat-shock protein 90 beta isoform (HSP90 beta) with cellular inhibitor of apoptosis 1 (c-IAP1) is required for cell differentiation. *Cell Death Different.*, **15**, 859–866.
4. Suzuki, S., Kulkarni, A.B., (2010). Extracellular heat shock protein HSP90beta secreted by MG63 osteosarcoma cells inhibits activation of latent TGF-beta1. *Biochem. Biophys. Res. Commun.*, **398**, 525–531.
5. Borkovich, K.A., Farrelly, F.W., Finkelstein, D.B., Taulien, J., Lindquist, S., (1989). hsp82 is an essential protein that is required in higher concentrations for growth of cells at higher temperatures. *Mol. Cell. Biol.*, **9**, 3919–3930.
6. Csermely, P., Schnaider, T., Soti, C., Prohaszka, Z., Nardai, G., (1998). The 90-kDa molecular chaperone family: structure, function, and clinical applications. A comprehensive review. *Pharmacol. Therap.*, **79**, 129–168.
7. Richter, K., Haslbeck, M., Buchner, J., (2010). The heat shock response: life on the verge of death. *Mol. Cell*, **40**, 253–266.
8. Schopf, F.H., Biebl, M.M., Buchner, J., (2017). The HSP90 chaperone machinery. *Nature Rev. Mol. Cell Biol.*, **18**, 345–360.
9. Zhao, R., Davey, M., Hsu, Y.C., Kaplanek, P., Tong, A., Parsons, A.B., et al., (2005). Navigating the chaperone network: an integrative map of physical and genetic interactions mediated by the hsp90 chaperone. *Cell*, **120**, 715–727.
10. Karagoz, G.E., Duarte, A.M., Akoury, E., Ippel, H., Biernat, J., Moran Luengo, T., et al., (2014). Hsp90-Tau complex reveals molecular basis for specificity in chaperone action. *Cell*, **156**, 963–974.

11. McClellan, A.J., Xia, Y., Deutschbauer, A.M., Davis, R.W., Gerstein, M., Frydman, J., (2007). Diverse cellular functions of the Hsp90 molecular chaperone uncovered using systems approaches. *Cell*, **131**, 121–135.
12. Picard, D., (2002). Heat-shock protein 90, a chaperone for folding and regulation. *Cell. Mol. Life Sci.: CMLS*, **59**, 1640–1648.
13. Pratt, W.B., Toft, D.O., (1997). Steroid receptor interactions with heat shock protein and immunophilin chaperones. *Endocrine Rev.*, **18**, 306–360.
14. Karagöz, G.E., Rüdiger, S.G., (2015). Hsp90 interaction with clients. *Trends Biochem. Sci.*, **40**, 117–125.
15. Bharadwaj, P.R., Dubey, A.K., Masters, C.L., Martins, R. N., Macreadie, I.G., (2009). Abeta aggregation and possible implications in Alzheimer's disease pathogenesis. *J. Cell. Mol. Med.*, **13**, 412–421.
16. Owen, M.C., Gnutt, D., Gao, M., Warmlander, S., Jarvet, J., Graslund, A., et al., (2019). Effects of in vivo conditions on amyloid aggregation. *Chem. Soc. Rev.*, **48**, 3946–3996.
17. Selkoe, D.J., Hardy, J., (2016). The amyloid hypothesis of Alzheimer's disease at 25 years. *EMBO Mol. Med.*, **8**, 595–608.
18. LaFerla, F.M., Green, K.N., Oddo, S., (2007). Intracellular amyloid-beta in Alzheimer's disease. *Nature Rev. Neurosci.*, **8**, 499–509.
19. Ripoli, C., Cocco, S., Li Puma, D.D., Piacentini, R., Mastrodonato, A., Scala, F., et al., (2014). Intracellular accumulation of amyloid-β (Aβ) protein plays a major role in Aβ-induced alterations of glutamatergic synaptic transmission and plasticity. *J. Neurosci.*, **34**, 12893–12903.
20. Li, M., Chen, L., Lee, D.H.S., Yu, L.-C., Zhang, Y., (2007). The role of intracellular amyloid β in Alzheimer's disease. *Prog. Neurobiol.*, **83**, 131–139.
21. Rushworth, J.V., Hooper, N.M., (2010). Lipid rafts: linking Alzheimer's amyloid-β production, aggregation, and toxicity at neuronal membranes. *Int. J. Alzheimer's Disease*, **2011**, 603052
22. Tofoleanu, F., Buchete, N.-V., (2012). Alzheimer Aβ peptide interactions with lipid membranes: fibrils, oligomers and polymorphic amyloid channels. *Prion*, **6**, 339–345.
23. Calderwood, S.K., Mambula, S.S., Gray, P.J., Theriault, J. R., (2007). Extracellular heat shock proteins in cell signaling. *FEBS Letters*, **581**, 3689–3694.
24. Horváth, I., Multhoff, G., Sonnleitner, A., Vígh, L., (2008). Membrane-associated stress proteins: more than simply chaperones. *Biochimica et biophysica acta*, **1778**, 1653–1664.
25. Fonte, V., Kapulkin, W.J., Taft, A., Fluet, A., Friedman, D., Link, C.D., (2002). Interaction of intracellular beta amyloid peptide with chaperone proteins. *Proc. Natl. Acad. Sci. USA*, **99**, 9439–9444.
26. Ansar, S., Burlison, J.A., Hadden, M.K., Yu, X.M., Desino, K.E., Bean, J., et al., (2007). A non-toxic Hsp90 inhibitor protects neurons from Abeta-induced toxicity. *Bioorg. Med. Chem. Lett.*, **17**, 1984–1990.
27. Chen, Y., Wang, B., Liu, D., Li, J.J., Xue, Y., Sakata, K., et al., (2014). Hsp90 chaperone inhibitor 17-AAG attenuates Abeta-induced synaptic toxicity and memory impairment. *J. Neurosci.: Off. J. Soc. Neurosci.*, **34**, 2464–2470.
28. Evans, C.G., Wisen, S., Gestwicki, J.E., (2006). Heat shock proteins 70 and 90 inhibit early stages of amyloid beta-(1–42) aggregation in vitro. *The Journal of biological chemistry.*, **281**, 33182–33191.
29. Takata, K., Kitamura, Y., Tsuchiya, D., Kawasaki, T., Taniguchi, T., Shimohama, S., (2003). Heat shock protein-90-induced microglial clearance of exogenous amyloid-beta1-42 in rat hippocampus in vivo. *Neurosci. Lett.*, **344**, 87–90.
30. Obermann, W.M., Sondermann, H., Russo, A.A., Pavletich, N.P., Hartl, F.U., (1998). In vivo function of Hsp90 is dependent on ATP binding and ATP hydrolysis. *J. Cell Biol.*, **143**, 901–910.
31. Adamcik, J., Mezzenga, R., (2012). Study of amyloid fibrils via atomic force microscopy. *Curr. Opin. Colloid Interface Sci.*, **17**, 369–376.
32. Banerjee, S., Sun, Z., Hayden, E.Y., Teplow, D.B., Lyubchenko, Y.L., (2017). Nanoscale dynamics of amyloid beta-42 oligomers as revealed by high-speed atomic force microscopy. *ACS Nano*, **11**, 12202–12209.
33. Drolle, E., Hane, F., Lee, B., Leonenko, Z., (2014). Atomic force microscopy to study molecular mechanisms of amyloid fibril formation and toxicity in Alzheimer's disease. *Drug Metabolism Rev.*, **46**, 207–223.
34. Watanabe-Nakayama, T., Ono, K., Itami, M., Takahashi, R., Teplow, D.B., Yamada, M., (2016). High-speed atomic force microscopy reveals structural dynamics of amyloid beta1-42 aggregates. *Proc. Natl. Acad. Sci. USA*, **113**, 5835–5840.
35. Downey, M.A., Giammona, M.J., Lang, C.A., Buratto, S.K., Singh, A., Bowers, M.T., (2019). Inhibiting and remodeling toxic amyloid-beta oligomer formation using a computationally designed drug molecule that targets Alzheimer's disease. *J. Am. Soc. Mass Spectrometry*, **30**, 85–93.
36. Hane, F., Tran, G., Attwood, S.J., Leonenko, Z., (2013). Cu (2+) affects amyloid-β (1–42) aggregation by increasing peptide-peptide binding forces. *PLoS One*, **8**, e59005-e
37. Lee, B.Y., Attwood, S.J., Turnbull, S., Leonenko, Z., (2018). Effect of varying concentrations of docosahexaenoic acid on amyloid beta (1(-)42) aggregation: an atomic force microscopy study. *Molecules*, **23**
38. Mangione, M.R., Vilasi, S., Marino, C., Librizzi, F., Canale, C., Spigolon, D., et al., (2016). Hsp60, amateur chaperone in amyloid-beta fibrillogenesis. *Biochim. Biophys. Acta*, **1860**, 2474–2483.
39. Walti, M.A., Steiner, J., Meng, F., Chung, H.S., Louis, J.M., Ghirlando, R., et al., (2018). Probing the mechanism of inhibition of amyloid-beta(1–42)-induced neurotoxicity by the chaperonin GroEL. *Proc. Natl. Acad. Sci. USA*, **115**, E11924–E11932.
40. Ojha, J., Masilamoni, G., Dunlap, D., Udoff, R.A., Cashikar, A.G., (2011). Sequestration of toxic oligomers by HspB1 as a cytoprotective mechanism. *Mol. Cell. Biol.*, **31**, 3146–3157.
41. Wallin, C., Hiruma, Y., Warmlander, S., Huvent, I., Jarvet, J., Abrahams, J.P., et al., (2018). The neuronal tau protein blocks in vitro fibrillation of the Amyloid-beta (Abeta) peptide at the oligomeric stage. *J. Am. Chem. Soc.*, **140**, 8138–8146.
42. Biancalana, M., Koide, S., (2010). Molecular mechanism of Thioflavin-T binding to amyloid fibrils. *Biochimica et biophysica acta*, **1804**, 1405–1412.
43. Cohen, S.I., Vendruscolo, M., Dobson, C.M., Knowles, T. P., (2011). Nucleated polymerization with secondary pathways. II. Determination of self-consistent solutions to growth processes described by non-linear master equations. *J. Chem. Phys.*, **135**, 065106

44. Cohen, S.I., Vendruscolo, M., Dobson, C.M., Knowles, T. P., (2012). From macroscopic measurements to microscopic mechanisms of protein aggregation. *J. Mol. Biol.*, **421**, 160–171.
45. Cohen, S.I., Linse, S., Luheshi, L.M., Hellstrand, E., White, D.A., Rajah, L., et al., (2013). Proliferation of amyloid-beta42 aggregates occurs through a secondary nucleation mechanism. *Proc. Natl. Acad. Sci. USA*, **110**, 9758–9763.
46. Knowles, T.P., Waudby, C.A., Devlin, G.L., Cohen, S.I., Aguzzi, A., Vendruscolo, M., et al., (2009). An analytical solution to the kinetics of breakable filament assembly. *Science (New York, NY).*, **326**, 1533–1537.
47. Meisl, G., Kirkegaard, J.B., Arosio, P., Michaels, T.C., Vendruscolo, M., Dobson, C.M., et al., (2016). Molecular mechanisms of protein aggregation from global fitting of kinetic models. *Nature Protocols*, **11**, 252–272.
48. Meisl, G., Yang, X., Hellstrand, E., Frohm, B., Kirkegaard, J.B., Cohen, S.I., et al., (2014). Differences in nucleation behavior underlie the contrasting aggregation kinetics of the Abeta40 and Abeta42 peptides. *Proc. Natl. Acad. Sci. USA*, **111**, 9384–9389.
49. Schönbrunn, E., Eschenburg, S., Luger, K., Kabsch, W., Amrhein, N., (2000). Structural basis for the interaction of the fluorescence probe 8-anilino-1-naphthalene sulfonate (ANS) with the antibiotic target MurA. *Proc. Natl. Acad. Sci.*, **97**, 6345.
50. Gasymov, O.K., Glasgow, B.J., (2007). ANS fluorescence: potential to augment the identification of the external binding sites of proteins. *Biochim. Biophys. Acta.*, **1774**, 403–411.
51. Bitan, G., (2006). Structural study of metastable amyloidogenic protein oligomers by photo-induced cross-linking of unmodified proteins. *Methods Enzymol.*, **413**, 217–236.
52. Bitan, G., Lomakin, A., Teplow, D.B., (2001). Amyloid beta-protein oligomerization: prenucleation interactions revealed by photo-induced cross-linking of unmodified proteins. *J. Biol. Chem.*, **276**, 35176–35184.
53. Mickler, M., Hessling, M., Ratzke, C., Buchner, J., Hugel, T., (2009). The large conformational changes of Hsp90 are only weakly coupled to ATP hydrolysis. *Nature Struct. Mol. Biol.*, **16**, 281–286.
54. Preston, G.W., Wilson, A.J., (2013). Photo-induced covalent cross-linking for the analysis of biomolecular interactions. *Chem. Soc. Rev.*, **42**, 3289–3301.
55. Krukenberg, K.A., Street, T.O., Lavery, L.A., Agard, D.A., (2011). Conformational dynamics of the molecular chaperone Hsp90. *Quart. Rev. Biophys.*, **44**, 229–255.
56. Li, J., Soroka, J., Buchner, J., (2012). The Hsp90 chaperone machinery: conformational dynamics and regulation by co-chaperones. *Biochim. Biophys. Acta*, **1823**, 624–635.
57. Lorenz, O.R., Freiburger, L., Rutz, D.A., Krause, M., Zierer, B. K., Alvira, S., et al., (2014). Modulation of the Hsp90 chaperone cycle by a stringent client protein. *Mol. Cell*, **53**, 941–953.
58. Shiau, A.K., Harris, S.F., Southworth, D.R., Agard, D.A., (2006). Structural analysis of E. coli hsp90 reveals dramatic nucleotide-dependent conformational rearrangements. *Cell*, **127**, 329–340.
59. Hellenkamp, B., Wortmann, P., Kandzia, F., Zacharias, M., Hugel, T., (2017). Multidomain structure and correlated dynamics determined by self-consistent FRET networks. *Nature Methods*, **14**, 174–180.
60. Coskuner, O., Murray, I.V., (2014). Adenosine triphosphate (ATP) reduces amyloid-beta protein misfolding in vitro. *J. Alzheimer's Disease: JAD*, **41**, 561–574.
61. Radli, M., Rudiger, S.G.D., (2018). Dancing with the diva: Hsp90-client interactions. *J. Mol. Biol.*, **430**, 3029–3040.
62. Oroz, J., Kim, J.H., Chang, B.J., Zweckstetter, M., (2017). Mechanistic basis for the recognition of a misfolded protein by the molecular chaperone Hsp90. *Nature Struct. Mol. Biol.*, **24**, 407–413.
63. Verba, K.A., Wang, R.Y., Arakawa, A., Liu, Y., Shirouzu, M., Yokoyama, S., et al., (2016). Atomic structure of Hsp90-Cdc37-Cdk4 reveals that Hsp90 traps and stabilizes an unfolded kinase. *Science (New York, NY).*, **352**, 1542–1547.
64. Kanno, D.M., Levitus, M., (2014). Protein oligomerization equilibria and kinetics investigated by fluorescence correlation spectroscopy: a mathematical treatment. *J. Phys. Chem. B*, **118**, 12404–12415.
65. Ali, M.H., Imperiali, B., (2005). Protein oligomerization: how and why. *Bioorg. Med. Chem.*, **13**, 5013–5020.
66. Picone, P., Nuzzo, D., Giacomazza, D., Di Carlo, M., (2020). β-Amyloid peptide: the cell compartment multi-faceted interaction in Alzheimer's disease. *Neurotoxicity Res.*, **37**, 250–263.
67. LaFerla, F.M., Green, K.N., Oddo, S., (2007). Intracellular amyloid-β in Alzheimer's disease. *Nature Rev. Neurosci.*, **8**, 499–509.
68. Oddo, S., Caccamo, A., Smith, I.F., Green, K.N., LaFerla, F. M., (2006). A dynamic relationship between intracellular and extracellular pools of Abeta. *Am. J. Pathol.*, **168**, 184–194.
69. Friedrich, R.P., Tepper, K., Rönicke, R., Soom, M., Westermann, M., Reymann, K., et al., (2010). Mechanism of amyloid plaque formation suggests an intracellular basis of Abeta pathogenicity. *Proc. Natl. Acad. Sci. USA*, **107**, 1942–1947.
70. Wirths, O., Multhaup, G., Bayer, T.A., (2004). A modified β-amyloid hypothesis: intraneuronal accumulation of the β-amyloid peptide – the first step of a fatal cascade. *J. Neurochem.*, **91**, 513–520.
71. Gotz, M., Wortmann, P., Schmid, S., Hugel, T., (2016). A multicolor single-molecule FRET approach to study protein dynamics and interactions simultaneously. *Methods Enzymol.*, **581**, 487–516.
72. Horcas, I., Fernández, R., Gómez-Rodríguez, J.M., Colchero, J., Gómez-Herrero, J., Baro, A.M., (2007). WSXM: A software for scanning probe microscopy and a tool for nanotechnology. *Rev. Sci. Instrum.*, **78**, 013705
73. Nečas, D., Klapetek, P., (2012). Gwyddion: an open-source software for SPM data analysis. *Cent. Eur. J. Phys.*, **10**, 181–188.
74. Lamour, G., Kirkegaard, J.B., Li, H., Knowles, T.P.J., Gsponer, J., (2014). Easyworm: an open-source software tool to determine the mechanical properties of worm-like chains. *Source Code Biol. Med.*, **9**, 16.
75. Luo, Jinghui, Wärmländer, Sebastian, Gräslund, Astrid, Abrahams, Jan Pieter, (2014). Alzheimer peptides aggregate into transient nanoglobules that nucleate fibrils. *Biochemistry*, **53**, 6302–6308. https://doi.org/10.1021/bi5003579.
76. Luo, Jinghui, Yu, Chien-Hung, Yu, Huixin, Borstnar, Rok, Kamerlin, Shina, Gräslund, Astrid, Abrahams, Jan Pieter, Wärmländer, Sebastian, (2013). Cellular Polyamines Promote Amyloid-Beta (Aβ) Peptide Fibrillation and Modulate the Aggregation Pathways. *ACS Chemical Neuroscience*, **4** (3), 454–462. https://doi.org/10.1021/cn300170x.